

Unraveling the Nanoscale Structure of Organic–Inorganic Hybrid Materials

Jacob Johnny,* Savarithai Jenani Louis Anandaraj, Carolin Mehrmann, Xin Wei, Ankita Das, Niklas Scheer, Yuke Yang, Walid Hetaba, Petra Ebbinghaus, Ulrich Simon, Rüdiger-A. Eichel, Florian Hausen, Holger Uphoff, Hans-Christoph Mertins, R. Kramer Campen, Yujin Tong, Martin Rabe, Walter Leitner, Alexis Bordet, and Marc Frederic Tesch*

Metal nanoparticles (NPs) immobilized on molecularly modified supports form versatile hybrid materials, offering extensive combinatorial flexibility and synergistic interactions between the organic and inorganic components, making them ideal for applications such as catalysis, and sensing. In catalysis, e.g., NPs-ionic liquid combinations are shown to enhance activity, selectivity, and recyclability compared to NPs alone systems, though typically used powder-based supports often hinder a detailed nanoscale structural analysis for an in-depth understanding due to undefined surfaces. Here, an approach is developed to transfer such a system onto well-defined surfaces for extended analysis, demonstrated on a model system composed of an imidazolium/NTf₂ ionic liquid and Ru NPs on Si. A comprehensive characterization suite is applied to probe the material properties at the nano- and macroscale including spatial arrangement, molecular orientation, surface homogeneity, hydrophilicity, and work function. The efficacy of the utilized approaches in obtaining a homogeneous ionic liquid monolayer decorated with Ru NPs of controlled distribution is demonstrated. It is identified that the particle deposition disturbs the conformational order of the molecular layer. The presented versatile methodological approach can be broadly expanded to multifunctional hybrid materials composed of metal NPs on molecularly modified supports, unlocking numerous possibilities for knowledge-driven and rational material design.

1. Introduction

Hybrid materials composed of metal nanoparticles (NPs) immobilized on molecularly modified surfaces (MMS) represent complex multicomponent systems where multiple functionalities are combined.^[1] Among these, NPs in combination with ionic liquids (ILs) are highly interesting owing to the versatile properties associated with both the inorganic (NPs) and organic (IL) components. In general, ILs possess a variety of tunable properties such as hydrophobicity/hydrophilicity, melting point, viscosity, and acidity/basicity, which makes systems composed of ILs highly attractive for specific applications, such as catalysis, sensors, and corrosion protection.^[1–5] When chemisorbed on a support, thereby forming a supported ionic liquid phase (SILP) and interacting with a catalytically active particle, the IL can enable catalyst recycling, enhanced stability, and facilitated product isolation. In addition, the application of IL as SILPs requires a significantly reduced amount

J. Johnny, S. J. L. Anandaraj, W. Hetaba, W. Leitner, A. Bordet, M. F. Tesch
Max Planck Institute for Chemical Energy Conversion
Stiftstr. 34–36, 45470 Mülheim, Germany
E-mail: jacob.johnny@cec.mpg.de; marc.tesch@cec.mpg.de

C. Mehrmann, A. Das, P. Ebbinghaus, M. Rabe
Max Planck Institute for Sustainable Materials
40237 Düsseldorf, Germany

 The ORCID identification number(s) for the author(s) of this article can be found under <https://doi.org/10.1002/admi.202500073>

© 2025 The Author(s). Advanced Materials Interfaces published by Wiley-VCH GmbH. This is an open access article under the terms of the [Creative Commons Attribution](https://creativecommons.org/licenses/by/4.0/) License, which permits use, distribution and reproduction in any medium, provided the original work is properly cited.

DOI: 10.1002/admi.202500073

X. Wei, U. Simon
Institute of Inorganic Chemistry
RWTH Aachen University
52074 Aachen, Germany

N. Scheer, R.-A. Eichel, F. Hausen
Forschungszentrum Jülich GmbH
Institute of Energy Technologies
IET-1 – Fundamental Electrochemistry
52425 Jülich, Germany

N. Scheer, R.-A. Eichel, F. Hausen
RWTH Aachen University
Institute of Physical Chemistry
Landoltweg 2, 52074 Aachen, Germany

Y. Yang, R. K. Campen, Y. Tong
Faculty of Physics
University of Duisburg-Essen
Lotharstraße 1, 47057 Duisburg, Germany

of ILs while still exploiting their unique features in the desired manner.^[6] SILPs are usually obtained by functionalizing a support material using an ionic liquid through chemisorption or physisorption thus creating a mono-, or multi-layer.^[7–9]

One common strategy of using the SILP is as a matrix for metal NPs immobilization, which opens a versatile molecular approach toward adaptive and multifunctional catalytic systems with tailor-made activity.^[3] In such combinations, the SILP is reported to influence the size^[10] and stability^[11,12] of NPs formed in their presence while bringing different types of functional groups in close contact with the metal.^[3] NPs-modified SILP (denoted from now on as NPs@SILP) systems have been already successfully applied to a variety of different catalytic reactions including hydrogenation/hydrodeoxygenation,^[13–15] the Suzuki reaction,^[16] and hydroformylation.^[17] The majority of the NPs@SILP systems use hydroxylated silica as the support material, which is cost-efficient and offers variable material properties such as pore size and shape.^[18] Although NPs@SILP systems based on powder supports have been widely studied and applied in catalytic reactions, a fundamental insight into the spatial arrangement of both SILP and NPs and the mutual influence on their spatial and electronic structure is still lacking. Such information would be however highly beneficial in facilitating a knowledge-based fine-tuning of their properties for targeted applications. Addressing these aspects would require advanced characterizations of the NPs@SILP systems, some of which are incompatible with the powder materials mainly due to their undefined geometry. In contrast, the use of flat supports would enable the application of additional analytical techniques to access complementary information, such as layer analysis by ellipsometry, determination of molecular orientations by attenuated total reflection infrared spectroscopy (ATR-IR), investigation of the local structure and reaction by sum frequency generation (SFG) spectroscopy,^[19] and Kelvin probe force microscopy (KPFM). The information gained from these studies on flat surfaces can ideally be transferred to better understand and fine-tune similar powder-based systems as well as to enhance their performance.

Herein, to close this knowledge gap by enabling a broader range of characterization on the NPs@SILP (and NPs@MMS in general), we used well-defined flat surfaces as supports. We report a facile synthesis procedure to obtain a molecularly modified commercial Si-wafer surface with an imidazolium-based IL through a chemical grafting approach and the subsequent decoration of the surface with ruthenium (Ru) NPs by DC magnetron sputtering. Characterization of the system is presented in detail by the application of a number of complementary analytical techniques which provide deeper insight into the spatial structure and the mutual interaction between different components in the NPs@SILP system.

H. Uphoff, H.-C. Mertins
Department of Engineering Physics
Münster University of Applied Sciences
Stegerwaldstrasse 39, 48565 Steinfurt, Germany
W. Leitner
Institut für Technische und Makromolekulare Chemie
RWTH Aachen University
52074 Aachen, Germany

2. Results and Discussion

2.1. Preparation of Wafer-Based SILPs and Characterization

A crucial prerequisite for this study was the transfer of the powder-based SILP synthesis approach to flat monocrystalline Si wafer surfaces, which is required to perform the aforementioned multitude of characterization techniques for exploring the component structure in NPs@SILP systems. To this end, the approach that is commonly used for powder-based systems^[1,20,21] was adapted and optimized iteratively to produce a chemisorbed well-defined, and stable SILP layer grafted onto the Si wafer surface (see Experimental Section S1.3, Supporting information for details). Modifying Si wafer surfaces by certain organic polymers, as well as shorter organic molecules in self-assembled monolayers (SAMs), is a well-studied approach.^[22,23] Also, the preparation of IL layers on flat surfaces obtained via self-assembly^[24] or spin coating^[25,26] was previously reported. In our study, we used single-side polished conductive p-type Si wafers with (100) orientation. First, to hydroxylate the Si wafer surface that can enable covalent grafting of the IL molecules, they were treated using piranha solution (1.5 mL H₂O₂ and 3.5 mL H₂SO₄) at 90 °C for 1 h. After thoroughly washing these wafers with deionized water and drying them under an Ar flow, they were transferred into a Schlenk flask containing 16 mm IL in toluene. The IL used is composed of imidazolium-based cations, termed here [C₄(C₃SiO_x)im]⁺, and NTF₂⁻ anions. The molecular grafting was performed at 95 °C for 18 h under an Ar atmosphere after which the wafers were ultrasonically washed three times using dichloromethane (DCM) to ensure the removal of any physisorbed IL molecules from the wafer. A schematic of the synthesis steps, alongside the resulting surface modification, is depicted in **Figure 1a**. The IL-modified Si wafer is hereafter denoted as SILP|Si.

After the grafting process, the molecularly modified Si surface was characterized in detail, to confirm the existence and homogeneity of the grafted IL as well as to determine the surface properties of the wafer without NPs. Due to the nature of the sample, i.e., being a molecular monolayer, a set of complementary techniques was utilized to obtain a comprehensive understanding of the SILP|Si surface.

In the first control step, *contact angle measurements* were conducted to confirm whether the modification approach led to the expected changes in hydrophobicity. **Figure 1b** shows the mean contact angles of the Si wafer in the pristine form without any pre-treatment, after piranha treatment, and after the molecular grafting of the IL with a representative image for each case in the inset. While the contact angle of the water drop on the pristine wafer is ≈90°, after piranha treatment, the contact angle reached the lower limits of an unambiguous determination (<ca 10°). This highly hydrophilic surface indicates a successful hydroxylation of the wafer surface by the piranha treatment.^[27] After the modification of wafers by the IL, the contact angle again increased to ≈70°. This significant difference in the contact angle before and after the IL grafting confirmed an efficient surface modification, which is underlined by the hydrophobic nature of the NTF₂⁻ anion^[28–30] present in the grafted IL molecules. It is also worth noting that an increase in the hydrophobicity is

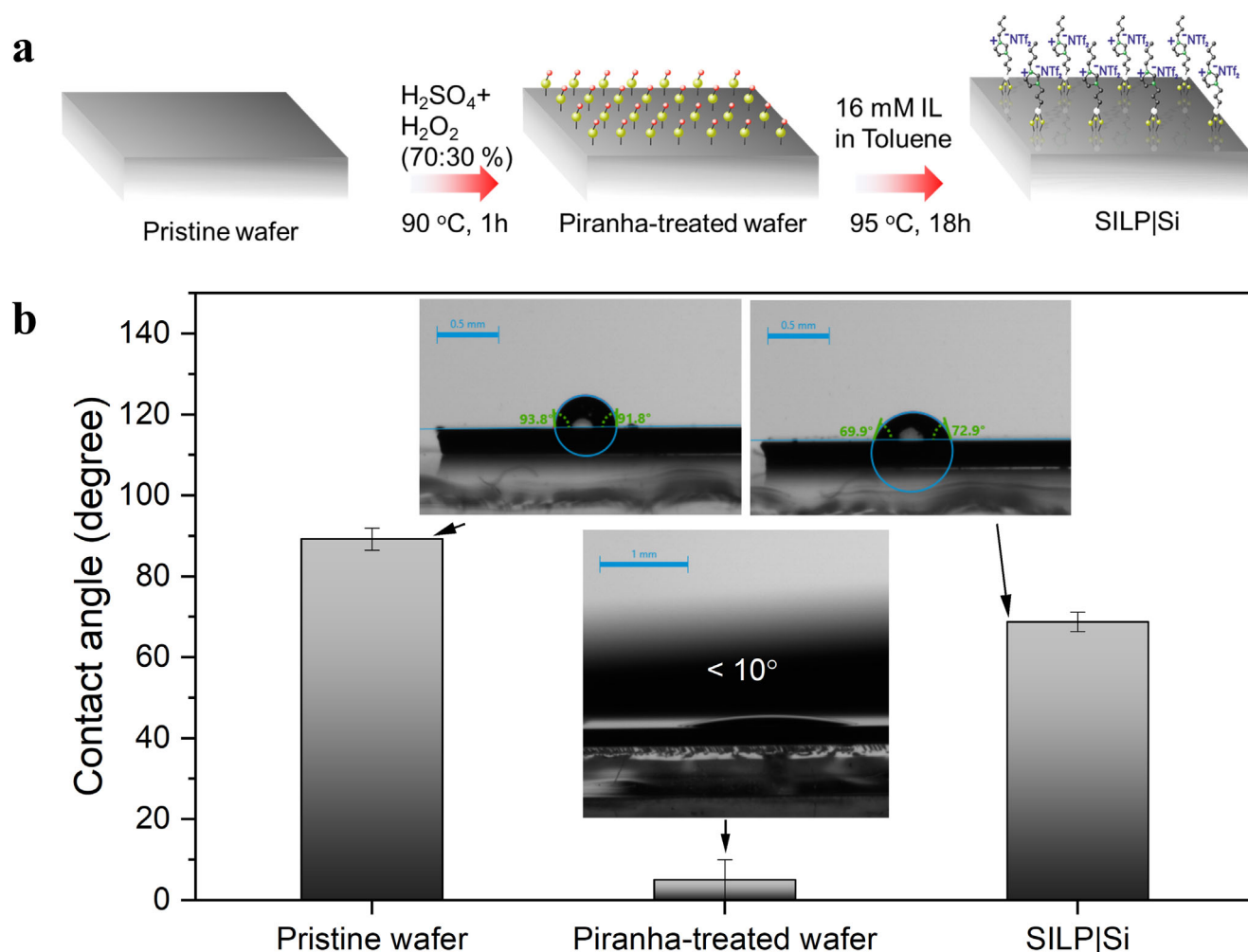


Figure 1. a) Schematic representation of the experimental procedure applied for the synthesis of SILP on Si wafer surfaces. b) Representative contact angle images of Si wafers in the pristine form, after piranha treatment, and IL grafting. Average contact angles from at least three independent measurements are presented with the standard deviations as error bars. In the case of the piranha-treated wafer, the depicted data of $5^{\circ} \pm 5^{\circ}$ only serves as visual guidance as the contact angles were not measurable by the in-built program due to the highly hydrophilic nature of the wafer surfaces.

expected from a well-ordered SAM in which all hydrophobic terminal chains point upward.

The thickness of the IL layer was subsequently evaluated using spectroscopic ellipsometry (SE). The measured data were fitted with optical models for the non-absorbing range of the SILP ($\lambda > 450\text{ nm}$). SILP|Si data was modeled by a simplified three-layer model. Typical results of the determined IL layer thicknesses for three samples measured on at least five different spots equally distributed over the surface show an average thickness of $1.59 \pm 0.4\text{ nm}$ (Figure S1, Supporting Information). Within the accuracy of this method, this result corresponds with the estimated length of the imidazolium-based cation of the IL ($\approx 1.2\text{ nm}$, Figure S2, Supporting Information). Thus, the formation of monolayers with ordered molecules in a relatively upright orientation (i.e., the alkyl chain axis being perpendicular to the substrate) is supported by these results. However, the data in Figure S1 (Supporting Information) further indicates a certain sample-to-sample variation in the measured average layer thicknesses.

SEM and EDX analyses can, in general, be used to characterize supported ionic liquid membranes,^[31,32] and to characterize different support materials modified by ILs^[33] when the loading of the IL is high enough. In contrast, the monolayer-like nature of the grafted IL molecules on Si supports, analyzed in this study, is not expected to yield noticeable structures, as evidenced by the high magnification SEM image on a SILP|Si sample shown in Figure S3a (Supporting Information). Nevertheless, SEM/EDX analysis can be applicable to detect any larger agglomerations present on the surface. IL agglomerations were occasionally observed on the surface as shown in Figure S3b (Supporting Information) with the corresponding EDX analysis detecting a higher abundance of the elements of the IL (Figure S3c–e, Supporting Information). However, the vast majority of the surface appeared smooth without any visual features or EDX signal of the IL elements above the detection limit, which is expected for the low material amount of a monolayer.

To confirm the formation and integrity of the IL layer on the sample surface, XPS analysis was undertaken, having the

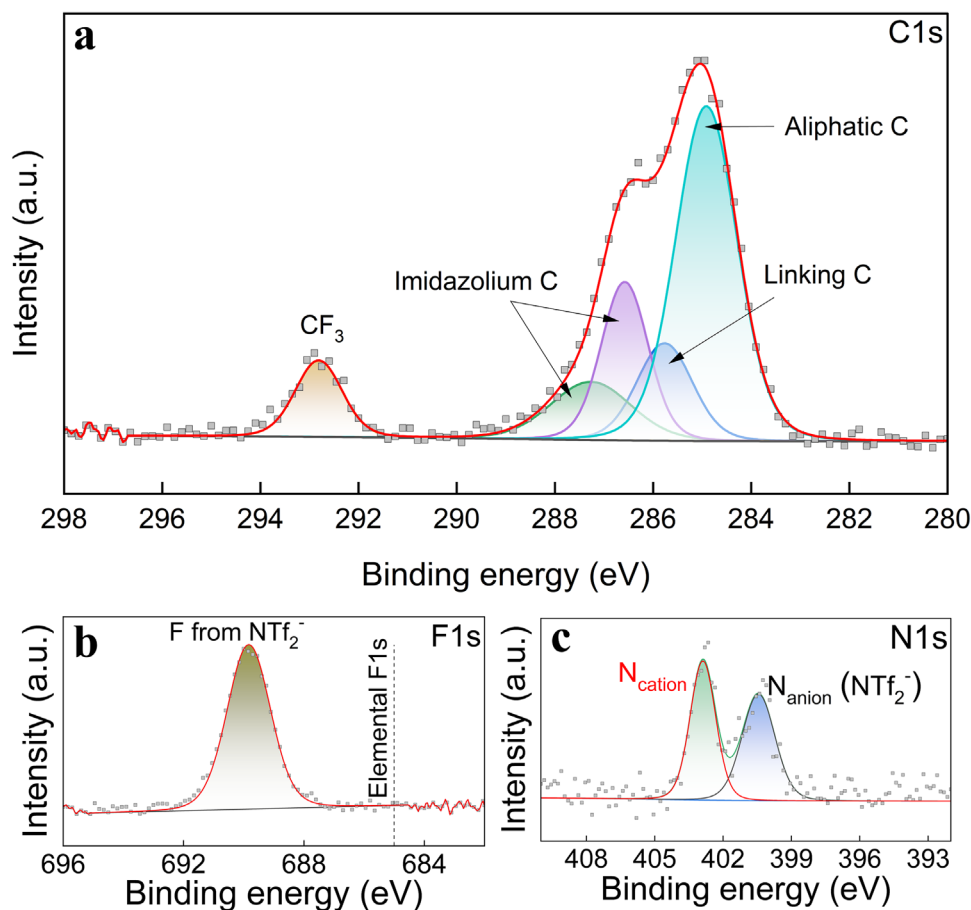


Figure 2. XPS spectra of a) C 1s b) F 1s and c) N 1s excitations from the SILP|Si sample.

particular advantage of surface sensitivity as well as element selectivity. **Figure 2** shows 1s XPS core level spectra of C, F, and N on the SILP|Si sample. The main C feature is located at a binding energy ≈ 286.0 eV and can be deconvoluted into four individual components including aliphatic, imidazolium, and linking carbons, in agreement with previously reported XPS data on a powder-based SILP for the same type of IL.^[10] An additional minor component can be detected at ≈ 293.0 eV, which corresponds to the carbon in CF_3 present in the NTf_2^- anion.^[34] The F1s feature at 690.0 eV possesses a significant shift from the elemental F (≈ 685.0 eV)^[35] as expected for fluorine in CF_3 ,^[36] and the N1s spectrum exhibits two major components located at ≈ 400.0 and 402.9 eV, which can be assigned to N contributions from the cationic and the anionic parts of the IL.^[36] Furthermore, in situ XPS (100 °C, 1 mbar H_2) studies confirmed the stability of the IL layer under conditions mimicking those in catalytic reactions (Figure S4, Supporting Information). Overall the XPS analysis not only confirms the presence of the IL layer on the Si wafer surface but also validates the desired chemical states of the cationic and the anionic parts of the corresponding IL.

To further evaluate the spatial homogeneity of the IL on the wafer surface, KPFM measurements were conducted. KPFM allows verification of changes in the work function induced by the covalently grafted IL molecules on the surface with a lateral resolution in the sub- μm scale.^[37,38] **Figure 3** shows the topog-

raphy and measured work functions of a pristine Si-wafer and SILP|Si. The topography of the Si-wafer, illustrated in **Figure 3a**, reveals a homogeneous surface without specific features as expected for a clean Si surface. In agreement with this, the simultaneously recorded work function (**Figure 3b**) is homogeneous over the entire measured surface. In comparison, the appearance of the topography obtained for the SILP|Si samples, shown in **Figure 3c**, is very similar. However, the work function, illustrated in **Figure 3d**, clearly verifies that the surface is strongly different in comparison with a pristine Si surface. Furthermore, the work function map proves the uniform distribution of the surface charge and thus, underlines the homogeneity of the IL grafting. As there is no overlap between the individual work function of the pristine Si surface and the SILP|Si (**Figure 3e**), the sample surfaces are clearly comprised of different chemical species. Small spherical structures, appearing as small white dots in the topography image, are present on the IL-modified surface in contrast to the pristine Si surface. These circular features are assigned to local aggregations of IL molecules as has been observed in similar polar monolayer systems.^[39] **Figure S5a** (Supporting Information) shows a higher resolution of the IL-modified surface, resolving the possible agglomerations in more detail. A line section across a representative dot (**Figure S5b**, Supporting Information) also reveals a height of ≈ 3 nm, which is in the dimension of molecular sizes of the IL.

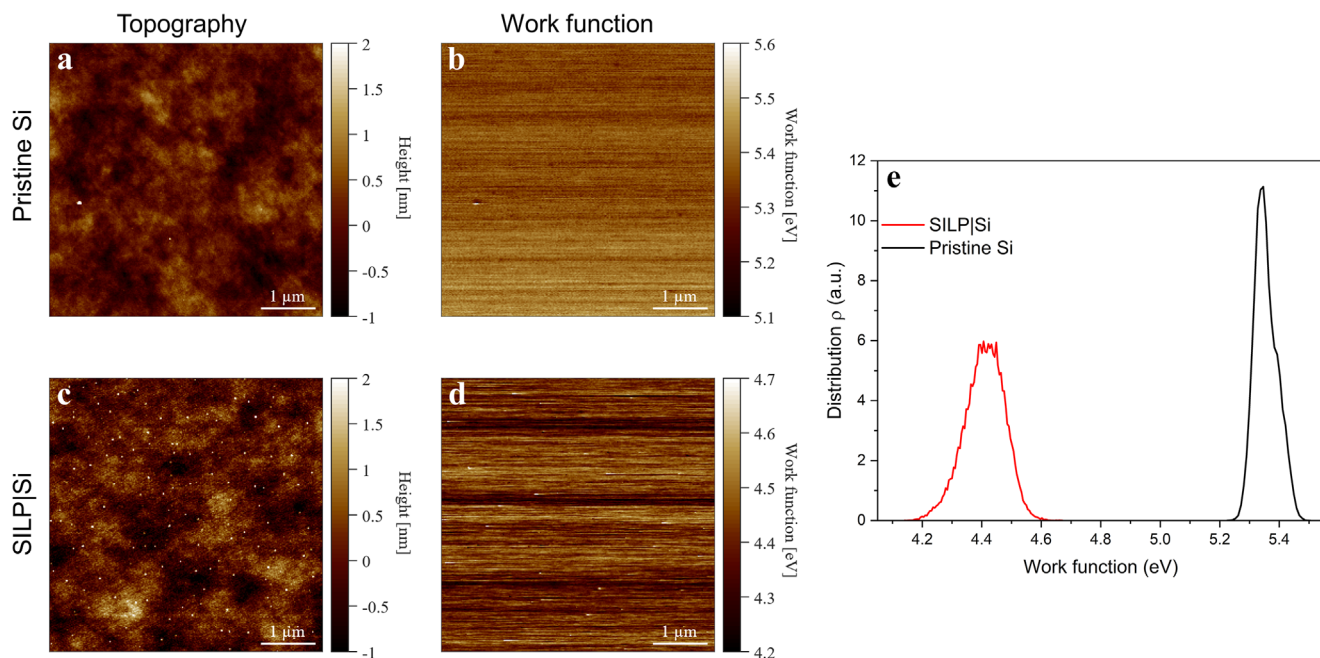


Figure 3. Kelvin probe force microscopy measurements. a) Topography and b) work function of pristine Si-wafer as well as after IL-modification (c and d, respectively). e) provides histograms of the work functions.

As an interim summary, the combination of the applied complementary techniques gives a comprehensive understanding of the SILP|Si system. While contact angle measurements confirmed the successful modification of the Si wafer surfaces by the IL molecules on the macro scale, the KPFM analysis proves full coverage of the surface on the microscale as no unmodified surface areas were identified. Further, SEM/EDX, and atomic force microscopy (AFM) reveal two types of inhomogeneities. First, areas of several μm diameter were found, appearing dark in SEM and yielding a strong EDX response of the elements present in the IL. These areas, however, were found only occasionally and probably originated from residual IL forming larger agglomerates during the drying process of DCM. Second, AFM showed small circular regions of height ≈ 3 nm indicating IL aggregation. However, these areas constitute only a marginal fraction of the overall surface as seen from Figure 3c, and it has to be noted that they were not found on all samples or sample regions. The formation of a minor fraction of multi-layers is also in agreement with the SILP layer thickness found slightly to be higher than the molecular length of the imidazolium backbone by ellipsometry. In agreement with the more hydrophobic character measured by contact angle analysis, this indicates in total an upright formation of the IL with the hydrophobic terminal chains pointing upward of full coverage and predominantly monolayer nature. Finally, the XPS analysis proves that both cations, as well as anions, stayed chemically intact after the molecular modification.

2.2. Deposition and Characterization of Ru NPs on Wafer-Based SILPs

To further functionalize the IL-modified Si wafers, e.g. to obtain catalytic activity, the surface is decorated with metallic NPs. For

the herein analyzed system, the NPs-SILP combination has already been successfully used as an efficient and adaptive catalyst for several hydrogenation reactions.^[1,40,41] Such systems often show unique characteristics emerging from the synergistic effect between the SILP and NPs in addition to enhanced catalyst recyclability due to SILP-induced NP stabilization against leaching.^[42] In our work, the NP material was chosen to be Ru, which is a commonly reported metal, used in combination with a variety of powder-based SILP systems due to its ability to dissociate hydrogen on the surface.^[12,43] It should be noted here that a first NP synthesis attempt, adopting the metal-organic approach, usually used on powders,^[1] was not successful on the flat Si wafer surface, due to excessive agglomeration of particles even after several iterative optimization attempts (Figure S6, Supporting Information). The significant differences in the geometry and surface roughness between the flat Si wafer surface and silica powder might be accounted for by the poor control over the size and distribution of Ru NPs formed on the wafer through the organometallic pathway. Hence, a magnetron sputtering deposition was applied as an alternative, as it was previously reported as an efficient method.^[44–46] A sputtering approach possesses the advantage that pure metal particles can be directly deposited in contrast to organic synthesis where size-controlling ligands have to be often used. In a recent work, Qadir et al. reported the synthesis of so-called naked Ru nanoparticles and clusters by sputtering in ionic liquid cages on powder-based supports for CO₂ hydrogenation.^[43] Alves et al. reported the synthesis of Ag NPs via sputtering in imidazolium-NTf₂ IL films of different alkyl chains yielding particles of sizes ≈ 60 nm.^[47] Synthesis of Au NPs was also reported by sputtering onto an IL-modified Si wafer obtaining 5–7 nm particles.^[48] The here obtained Ru NPs on the SILP|Si are comparatively smaller (3 nm) in size and homogeneously distributed on the surface, as discussed below.

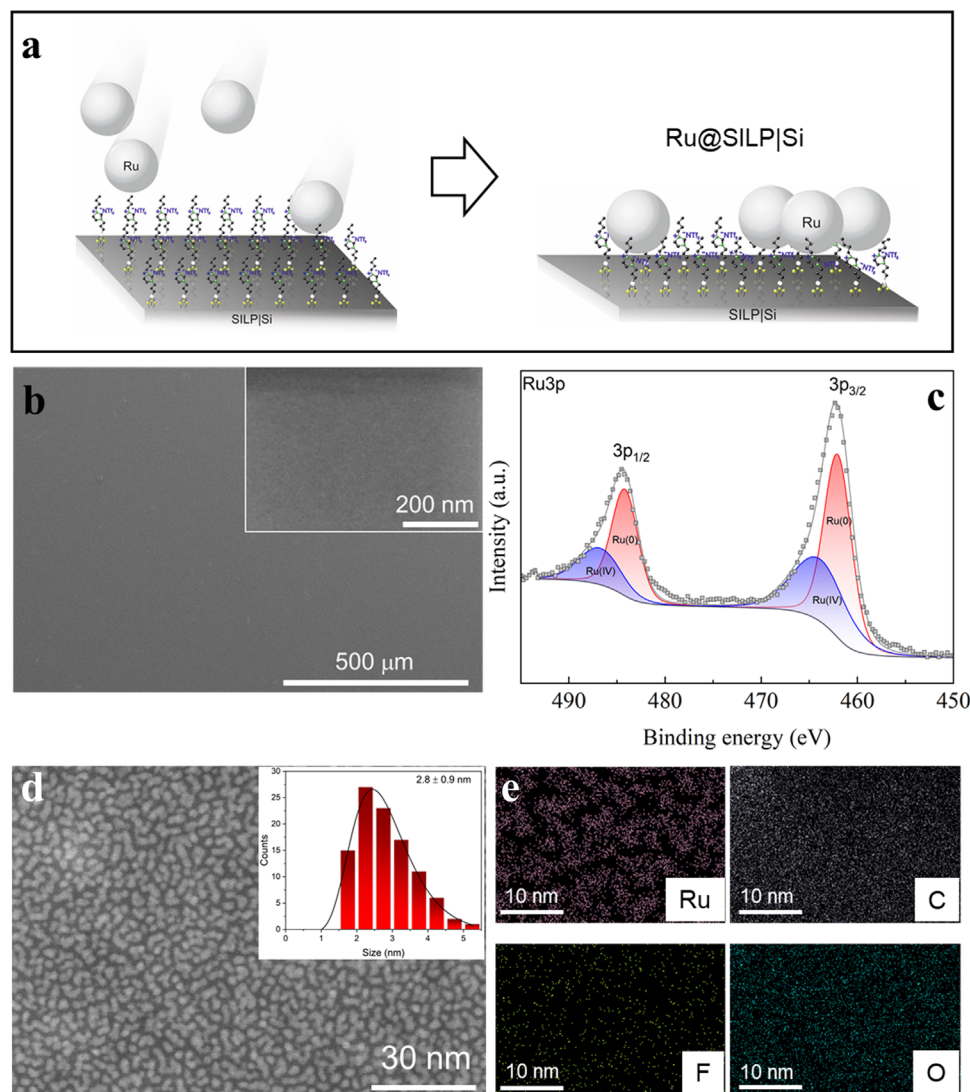


Figure 4. a) Schematic of the magnetron sputtering deposition of Ru NPs onto SILP|Si substrates and the expected Ru@SILP|Si structure b) Low magnification SEM image showing the surface of Ru@SILP|Si with the magnified area shown in the inset c) XPS Ru3p spectra taken on the Ru@SILP|Si sample. d) High-angle annular dark-field STEM image showing the distribution of sputtered Ru particles on a SILP|Si substrate with average size distribution fitted with a log-normal function in the inset. e) EDX maps for Ru, C, F, and O on the Ru@SILP|Si sample.

In our case, the Ru NPs deposition was realized via magnetron sputtering in DC mode under mild conditions (i.e., at a power of 100 W for 2 s) onto the SILP|Si wafer surfaces. These sputter parameters were chosen after iterative testing (Table S1, Supporting Information), showing that higher sputter durations lead to the formation of a complete coverage of the SILP|Si surface by a Ru layer (noted visually by a gradient color change and corresponding EDX measurements as shown in Figure S7, Supporting Information).

A schematic representation of the NP deposition on the SILP|Si via magnetron sputtering is shown in Figure 4a. According to a similar approach described in the literature, the sputtering is expected to decorate the SILP|Si surface with <10 nm Ru NPs.^[48] Low magnification SEM images with low acceleration voltage (1.0 kV) to increase surface sensitivity indicate no larger agglomerates of Ru on the examined samples (represent-

tatively shown in Figure 4b) as well as in a magnified area on the surface (inset of Figure 4b). To probe the presence of Ru on the surface, EDX measurements were performed on several randomly chosen spots. Indeed, the presence of small amounts of Ru was detected on each analyzed spot (Figure S8, Supporting Information) indicating a uniform Ru coverage on the entire surface. XPS analysis on the Ru NPs-decorated SILP|Si (denoted here as Ru@SILP|Si) samples corroborated the EDX results. As shown in Figure 4c, the Ru3p spectrum exhibits two distinct features corresponding to the spin-orbit split $3p_{1/2}$ and $3p_{3/2}$ core levels. These features are comprised of each two peaks, one at ≈ 484.2 and ≈ 462.0 eV, respectively, from metallic Ru^[35] whereas those located at ≈ 464.4 and 487.1 eV are assigned to a slight contribution of Ru(IV) as present in RuO₂.^[49] As for the SILP|Si samples, occasionally spherical structures of ≈ 15 – 20 nm size were found on the surface when analyzed by SEM with enhanced

surface sensitivity as shown in Figure S9 (Supporting Information). It should be noted that the white dots appearing on the SEM images shown in Figure S8 and S9 (Supporting Information) resemble those identified in the AFM (Figure 3c) analysis of the SILP|Si indicating random IL aggregations.

To characterize the deposited Ru NPs at a particle level, TEM analysis was conducted. Since an electron transparent substrate is needed for TEM, the SILP and NP synthesis procedure was transferred onto TEM frames consisting of 30 nm thick Si-membranes (see Experimental Section for details). The IL grafting and Ru NPs sputtering procedures were kept identical with the only difference being that ultrasonication was avoided in the washing step in DCM after the SILP synthesis as it leads to the immediate breaking of the thin Si window.

Figure 4d shows the STEM images taken in high-angle annular dark field (HAADF) mode on the NP-modified SILP|Si TEM windows. Indeed, the results confirm a uniform distribution of irregular particles with the size of most particles in the range of 2–4 nm with an estimated mean size of 2.8 ± 0.9 nm (measured manually for more than 100 particles using the ImageJ software package), thus making them highly comparable to the typical NP sizes achieved through organometallic synthesis when powder-based supports are used.^[50] Corresponding EDX maps of Ru, C, F, and O confirm these particles to be Ru (Figure 4e). Notably, the sputtering process applied here did not yield a completely closed layer of Ru on the SILP and the estimated surface coverage of Ru NPs is found to be ≈ 50 –60%. EDX maps confirmed that the observed bright-appearing structures stem from a Ru-rich phase. The IL elements (e.g., F) could not be clearly detected, which we attribute to the short plasma treatment that had to be applied to the TEM samples before the high-resolution EDX analysis, due to an otherwise strong carbon accumulation during the measurement.

To elucidate the effect of the SILP layer on the Ru particle formation, Ru was also sputter-deposited onto a pristine Si window (without the SILP layer, hereafter denoted as Ru@Si) as a reference. Under similar conditions, Ru sputtering onto a pristine Si wafer resulted in the formation of more interconnected Ru NPs (Figure S10, Supporting Information) in comparison with the particles formed on a SILP|Si surface, resulting in an estimated mean size of 5.1 ± 3.2 nm. The differences in particle formation are likely attributed to the absence of the IL layer, as a SILP can enhance NP stabilization in powder-based supports, which even can be tuned easily by varying the type of the IL.^[10] The stability of imidazolium-based NPs@SILP materials under solution phase catalytic conditions (e.g., organic solvents, 100–200 °C, 20–50 bar H_2) was investigated in many studies by our group and proved excellent (no substantial leaching nor structural change) under both batch and continuous flow conditions.^[10,42,51] Further interactions between the NP and SILP are discussed in the following section.

2.3. Mutual Interaction Between SILP and Ru NPs

The interaction/mutual influence of the SILP layer and Ru NPs is key information that can be used for designing NPs@SILP systems with defined properties and is studied in the following. SE was used to examine the Ru@SILP|Si, and Ru@Si samples to

compare the change in layer thicknesses with that of SILP|Si. An exemplary data set and the optical model fit are shown in Figure 5a. Especially $\Delta(\lambda)$ is very sensitive to thin films and decreases with increasing thin film thickness, as was observed for Si and SILP|Si. The change of $\Psi(\lambda)$ in the UV, especially recognizable between 320 and 350 nm, indicates an extinction coefficient $k > 0$ in this region^[52] that is assigned to the UV absorbance inherent to imidazolium cations.^[53]

Similar to the TEM analysis, alongside the Ru@SILP|Si, also a corresponding Ru@Si reference system was measured. Ellipsometry is sensitive to a SILP interlayer as long as the sputtered metal layer is thin enough to let light pass to the substrate.^[54] Optical model simulations (Figure S11, Supporting Information) indicate that Ru layers below 40 nm thickness are translucent and yield information on the SILP underneath. On Ru@Si, a thin metal layer absorbing in the whole spectral range was formed, confirmed by the increase of $\Psi(\lambda)$, the decrease in $\Delta(\lambda)$, and changes in slope compared to bare Si (Figure 5a). Exactly the same trends are observed for Ru@SILP|Si with respect to SILP|Si. Furthermore, $\Delta(\lambda)$ of Ru@SILP|Si is significantly reduced with respect to Ru@Si, which confirms the presence of the SILP interlayer between Ru and Si.

Due to the difficulties in the determination of the complex refractive index N_{Ru} (cf supporting discussion), for Ru@SILP|Si and Ru@Si, a self-consistent global model was devised that gives access to the SILP thickness or N after sputtering (Figure 5a inset). The thickness of the SILP layer is slightly altered after Ru sputtering. For the curves modeled with a constant n_{SILP} shown in Figure 5a, d_{SILP} apparently increases from 2.1 nm before sputtering to 2.4 nm after sputtering. However, it must be considered that thickness and refractive index are closely correlated for such thin films (see Figures S12 and S13, Supporting Information, and Experimental Section), hence an alternative and much more likely interpretation of this experimental result is a constant (or even decreased) d_{SILP} with an increased n_{SILP} due to a compression of the SILP and/or indentation of the metal into the SILP. A clear distinction between these two models is currently not possible due to the ambiguity of the Ru optical properties discussed in the Supporting information. Nevertheless, the analysis of the SE data clearly shows that a continuous and intact intermediate SILP layer is present between the Ru metal and Si/SiO₂ after sputtering.

To corroborate the observation of the homogeneity of the Ru NPs deposited via sputtering on the SILP|Si, KPFM was used. It was found that Ru NPs on SILP|Si indeed show a homogenous topography and work function map, depicted in Figure 5b–d. In the topography image, the previously mentioned spherical structures of a very few 10 nm diameter are again visible as white dots which is in line with the SEM images taken after the Ru NPs deposition (Figure S9, Supporting Information). Because of the lower KPFM resolution, individual Ru NPs structures are not clearly detected, although indicated in the work function map, cf Figure 5c. The histogram in Figure 5d shows a broader distribution of the work function in comparison to those of the pristine Si wafer and the SILP|Si surface as provided in Figure 3e. These work function differences further demonstrate the successful deposition of Ru NPs by means of sputtering and the corresponding alteration of the surface properties. Alongside the change in surface work function, also a change in the surface wetting behavior

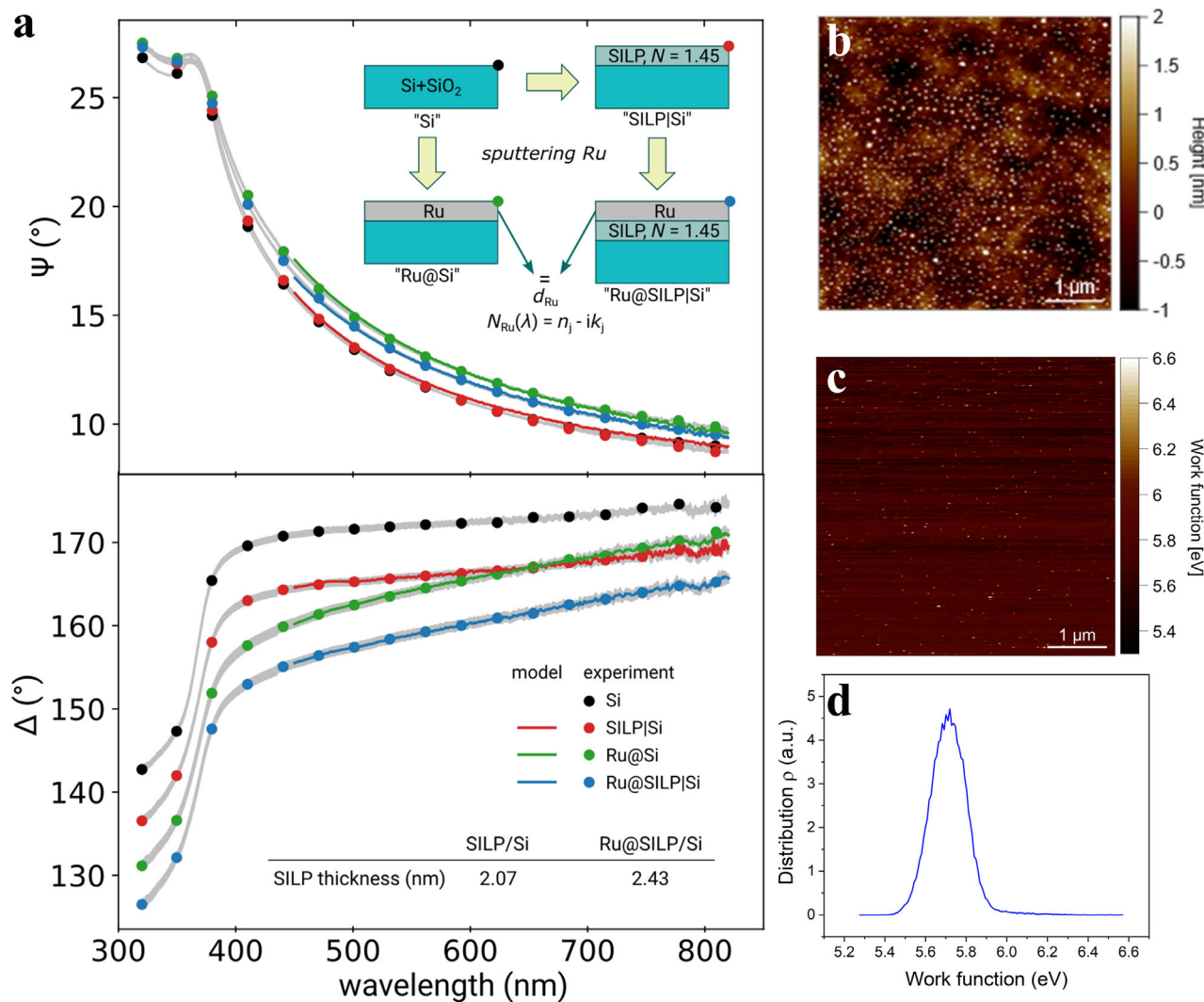


Figure 5. a) Spectroscopic ellipsometry on Si, SILP|Si, Ru@Si, and Ru@SILP|Si. The inset depicts the global analysis model used. b) Topography of Ru NPs deposited via sputtering under mild conditions (100 W, 2 s) on the SILP-modified Si-wafer sample exhibiting a smooth surface with some structures on top. c) work function map of the Ru NPs modified SILP|Si surface showing a homogeneous distribution and some small structures, exhibiting an enlarged work function. The histogram provided in d) shows a broader distribution in comparison to the SILP|Si and pristine Si surface as shown in Figure 3e.

was observed after the NPs deposition. Contact angle measurements were conducted on the Ru@Si and Ru@SILP|Si which demonstrated similar contact angles (85° for Ru@Si and 86° for Ru@SILP|Si) indicating that the surface wettability is more dominated by the Ru NPs than the SILP layer (Figure S14, Supporting Information). The obtained contact angle values are slightly higher in comparison with the SILP|Si surface (70°) thus the surface becomes slightly more hydrophobic after being decorated with Ru NPs.

The influence of Ru NPs sputtering onto SILP|Si was further investigated by ATR-IR (Figure 6a). In the lower wavenumber range, strong baseline deviations were observed that are ascribed to variations in SiO₂ thickness between the sample and the reference (piranha cleaned Si wafer). These make an analysis of the spectra below 1800 cm⁻¹ very challenging, which is therefore omitted for ATR-IR analysis. In the range above 2700 cm⁻¹

typical patterns of overlapping bands were observed that can be assigned to C–H stretching vibrations of the chemisorbed [C₄(C₃SiO_x)im]⁺ cation. These bands are mainly assigned to two groups, the first one from 3000 to 2800 cm⁻¹ is assigned to the antisymmetric and symmetric C–H stretching modes (C–H ν_{as} , C–H ν_s) of the alkyl chains (cf Table 1). The other peak in the range of 3200–3000 cm⁻¹ corresponds to the C–H stretching modes of the imidazolium ring.^[55] The deposition of Ru has a noticeable effect on both the positions and the peak width of the aliphatic C–H stretching vibrations (Figure 6a and Table 1), which are well known to reflect the order of chains in aliphatic SAMs.^[56] The positions of ν_{as} CH₂ and ν_s CH₂ at 2918 and 2849 cm⁻¹ conform with highly ordered aliphatic chains with all-trans conformations. Upon Ru sputtering, both CH₂ stretching bands increase slightly in frequency and broaden, which indicates a loss of conformational order due to an increasing

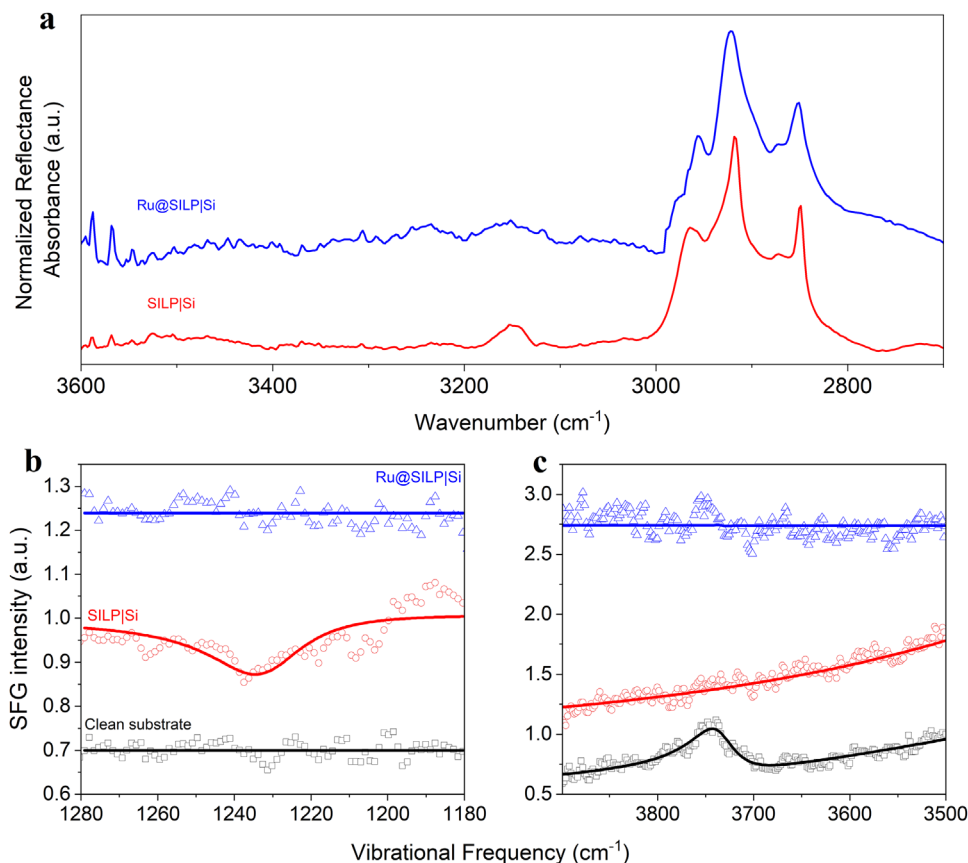


Figure 6. a) ATR-IR spectra of SILP|Si and Ru@SILP|Si. SFG spectra in b) C–F, and c) O–H stretching frequency regions for three different samples: clean substrate (black squares), SILP|Si substrate (red circles), and Ru@SILP|Si (blue triangles). The solid lines are the fit to the experimental results using a Lorentzian lineshape model.^[61]

population of gauche defects. Also, the antisymmetric C–H₃ stretching vibration at 2965 cm⁻¹ is strongly influenced by sputtering, although the decrease in frequency is not well understood yet. Furthermore, the position of the ν_{Ring} C–H at ≈ 3152 cm⁻¹ indicates that the imidazole ring is not strongly bound by the NTF₂ anion.^[57] Further, the position of this band is only weakly influenced by Ru sputtering although it also broadens noticeably.

To obtain an even deeper insight into the NP-SILP interactions in the Ru@SILP|Si system, we utilized SFG spectroscopy. Figure 6b,c shows the vibrational SFG spectra for clean Si substrate (black squares), SILP|Si (red circles), and NP@SILP|Si (blue triangles) in two different IR frequency regions. In Figure 6b, the IR frequency was tuned to excite the C–F stretching region. A clear resonant feature centered at ≈ 1232 cm⁻¹ can be observed. This is known to be related to the

CF₃ groups of the NTF₂ anions (note: different from FTIR measurements, the resonant features in SFG can appear as peaks, dips, or even bipolar. See our previous publication for more information^[58]). Interestingly, after NPs deposition, the peak disappears, suggesting that the molecular ordered structure has been disturbed.

Figure 6c covers O–H stretching and shows only for the Si substrate a narrow feature centered ≈ 3735 cm⁻¹, which can be assigned to the surface O–H stretching of the hydroxy group after the piranha treatment. Such a feature has been observed on many oxides under ambient conditions.^[59] After the surface modification by the SILP and also after modification by Ru NPs, this feature completely disappears (red curve in Figure 6c), proving the covalent bond formation during the SILP synthesis process. In addition to the information about pure vibrational modes, the line shape of vibrational SFG signals encompasses phase information, enabling the determination of the relative orientation of dipole moments in the moieties of interest, provided the nonresonant background is relatively large, as observed in the current study. Generally, a peak-shaped signal (e.g., the O–H group in Figure 6c) indicates that the dipole moment of the vibrational group is in phase with the electric dipole moment of the surface. Conversely, a dip-like shape (e.g., CF₃ in Figure 6b) suggests an opposite orientation of the vibrational group's dipole moment relative to the electric dipole moment of the surface.

Table 1. Maxima of experimental C-H ATR-IR bands and assignments.

SILP Si	Ru@SILP Si	Assignment
3151 cm ⁻¹	3152 cm ⁻¹	ν_{Ring} C–H
2965 cm ⁻¹	2955 cm ⁻¹	ν_{as} CH ₃
2918 cm ⁻¹	2922 cm ⁻¹	ν_{as} CH ₂
2849 cm ⁻¹	2851 cm ⁻¹	ν_{s} CH ₂

When the polarity direction of the surface is known, the absolute orientation can be determined accordingly.^[60] Here, if we assume that the surface electronic dipole moment is oriented toward the substrate because of the O-terminated surface, it follows that the O—H is directed toward the air, while the C—F bond is oriented toward the substrate. Additional vibrational SFG measurements were performed in the C—H stretching region (see Figure S15, Supporting Information). The observed general trend of red-shifted peaks and the transition from structural order to disorder upon deposition of Ru NPs is consistent with the findings from the ATR-IR measurements. Unfortunately, a closer analysis by XPS of the structural changes in the SILP after Ru particle deposition was not possible because the coverage of the Ru NPs hindered the detection of the SILP components. It is also worth noting here that the SILP layer has no apparent influence on the chemical behavior of sputter-deposited Ru NPs as the Ru3p high-resolution XPS spectra obtained on the SILP/Si resembles that obtained on a pristine Si wafer (Figure S16, Supporting Information).

Altogether the ATR-IR and SFG measurements provide comprehensive insight into IL layer grafted onto the Si wafer as well as changes induced by the Ru NPs deposition. Even though SFG and XPS measurements could not prove the presence of the IL layer after being decorated with Ru NPs, ATR-IR, and SE confirm the existence of the molecular layer on the Ru@SILP/Si sample. Given the potential of these techniques and their surface sensitivity, the approach presented herein with Si-wafer-based NPs@SILP systems is found to be highly beneficial which would otherwise not be applicable on powder-based NPs@SILP systems. The analysis of Ru@SILP/Si, Ru@Si, and SILP/Si samples suggests that the interaction between SILP and Ru is primarily structural. TEM reveals that the presence of SILP leads to smaller, less interconnected Ru NPs. SE confirms the integrity of the IL interlayer after sputtering, while ATR-IR and SFG indicate that Ru distorts the conformational order of the SILP and increases the amount of gauche defects. However, XPS analysis shows that the chemical state of Ru remains unchanged when comparing both configurations. Additionally, the hydrophobicity of the system, at 50–60% Ru coverage, appears to be dominated by the Ru NPs, with no significant influence from the SILP interlayer. These findings provide an initial nanoscale view of NPs@SILP systems on flat surfaces. While focused on a specific model system, the approach can be extended to other NPs@SILP configurations, given that various types of ILs have been successfully grafted onto powder-based silica supports,^[1,62] and NP decoration via sputtering is adaptable to different materials, as demonstrated, e.g., for Au NPs.^[48] Since the sputtering method is independent of the modified support, it offers broad applicability. However, each new system requires thorough analysis, with systematic parameter variation to distinguish individual and universal aspects of NP formation, molecular distortions, and NP-molecule interactions.

3. Conclusion

In summary, we demonstrated a facile approach to modify Si wafer surfaces with IL having a monolayer-like thickness which was subsequently decorated by Ru NPs. This transfer of the NP@SILP system from conventional powder-based supports

onto flat surfaces enabled an extended in-depth characterization of the individual nanoscale components thus providing insight into the spatial distribution, surface properties, and molecular orientations of the grafted SILP layer and the mutual interaction with the Ru NPs and their formation. By utilizing a set of complimentary characterization techniques, we first verified the existence of the thin IL layer on the modified Si wafers. In particular, we confirmed the monolayer-like thickness and predominantly homogeneous surface coverage through ellipsometry and KPFM measurements, which are both techniques not feasible on powder-based SILPs. By further transferring the NP@SILP system to a TEM-compatible Si membrane, we identified that the imidazolium/NTf₂⁻ IL influences the formation of the magnetron-sputtered Ru NPs yielding smaller structures in the presence of the SILP with no apparent chemical changes. Using ATR-IR and SFG spectroscopy, we identified a likely perpendicular orientation relative to the substrate of parallelly aligned alkyl chains, with the anions adopting an opposing orientation. Upon NPs deposition, SE revealed a chemically intact IL layer interlayered between the substrate and particles. However, the deposition of NPs disturbed the ordered molecular arrangement, leading to the loss of conformational order under the given conditions. These results demonstrate that the approach presented herein for transferring such systems from powder to flat Si wafers opens new pathways toward a more detailed understanding of such complex systems. In addition to the techniques presented herein, the arrangement of IL molecules on well defined flat surfaces also enables further analysis techniques, such as angle-resolved XPS (AR-XPS), as reported by Lockett et al.,^[63] which can provide even more information about the spatial arrangement but was beyond the scope of this study. Furthermore, structure-property-performance correlations might be also obtained under in situ *operando* conditions. Finally, the versatile approach and workflow showcased here for NPs@SILP systems are easily transferrable to the large family of NPs@MMS materials. This approach can be utilized for detailed studies on systematic variation in molecular modifiers, and NP materials, facilitating the fundamental understanding of such systems and enabling a knowledge-based design and optimization for technical applications.

Supporting Information

Supporting Information is available from the Wiley Online Library or from the author.

Acknowledgements

The authors acknowledge financial support by the Max Planck Society and Deutsche Forschungsgemeinschaft (DFG, German Research Foundation), under Germany's Excellence Strategy – Exzellenzcluster 2186 “The Fuel Science Center,” no. 390919832. MR's work is funded by DFG under Germany's Excellence Strategy EXC 2033 – 390677874 – RESOLV. John-Tommes Krzeslack and Norbert Pfänder are acknowledged for their support in XPS and TEM measurements, respectively. Hans Bongard is acknowledged for initial SEM/EDX analysis at MPI KoFo. F.H. and N.S. thank Ivan Soldo for the KPFM measurements. This work was also funded by DFG project no. 388390466-TRR 247, Project B03.

Conflict of Interest

The authors declare no conflict of interest.

Data Availability Statement

The data that support the findings of this study are available from the corresponding author upon reasonable request.

Keywords

microscopy, molecularly modified surfaces, molecule-nanoparticle interaction, nanoparticles, sum frequency generation spectroscopy

Received: January 24, 2025

Revised: March 24, 2025

Published online:

- [1] A. Bordet, W. Leitner, *Acc. Chem. Res.* **2021**, *54*, 2144.
- [2] P. McNeice, P. C. Marr, A. C. Marr, *Catal. Sci. Technol.* **2021**, *11*, 726.
- [3] G. Moos, M. Emondts, A. Bordet, W. Leitner, *Angew. Chem., Int. Ed.* **2020**, *59*, 11977.
- [4] C. Verma, E. E. Ebenso, M. Quraishi, *J. Mol. Liq.* **2017**, *233*, 403.
- [5] M. C. Buzzeo, C. Hardacre, R. G. Compton, *Anal. Chem.* **2004**, *76*, 4583.
- [6] Ambika, P. P. Singh, *Curr. Org. Synth.* **2022**, *19*, 905.
- [7] P. Virtanen, T. O. Salmi, J.-P. Mikkola, *Top. Catal.* **2010**, *53*, 1096.
- [8] R. M. F. Bento, C. A. S. Almeida, M. C. Neves, A. P. M. Tavares, M. G. Freire, *Nanomaterials*. **2021**, *11*, 11102542.
- [9] R. Meijboom, M. Haumann, T. E. Müller, N. Szesni, In *Supported Ionic Liquids*, Wiley-VCH Verlag GmbH & Co, Weinheim **2014**, pp. 75–94.
- [10] A. Bordet, G. Moos, C. Welsh, P. Licence, K. L. Luska, W. Leitner, *ACS Catal.* **2020**, *10*, 13904.
- [11] V. M. Chernyshev, O. V. Khazipov, D. B. Eremin, E. A. Denisova, V. P. Ananikov, *Coordinat. Chem. Rev.* **2021**, *437*, 213860.
- [12] K. L. Luska, P. Migowski, W. Leitner, *Green Chem.* **2015**, *17*, 3195.
- [13] K. L. Luska, P. Migowski, S. El Sayed, W. Leitner, *Angew. Chem.* **2015**, *127*, 15976.
- [14] K. L. Luska, P. Migowski, S. El Sayed, W. Leitner, *ACS Sustain. Chem. Engin.* **2016**, *4*, 6186.
- [15] L. Offner-Marko, A. Bordet, G. Moos, S. Tricard, S. Rengshausen, B. Chaudret, K. L. Luska, W. Leitner, *Angew. Chem.* **2018**, *130*, 12903.
- [16] M. Gruttadauria, L. F. Liotta, A. M. P. Salvo, F. Giacalone, V. La Parola, C. Aprile, R. Noto, *Adv. Synth. Catal.* **2011**, *353*, 2119.
- [17] A. Weiß, M. Munoz, A. Haas, F. Rietzler, H.-P. Steinrück, M. Haumann, P. Wasserscheid, B. J. M. Etzold, *ACS Catal.* **2016**, *6*, 2280.
- [18] A. Wolny, A. Chrobok, *Molecules*. **2022**, *27*, 5900.
- [19] X. Gong, R. K. Campen, Y. Tong, *J. Phys. Chem. C*. **2023**, *127*, 16615.
- [20] B. Xin, J. Hao, *Chem. Soc. Rev.* **2014**, *43*, 7171.
- [21] S. Minko, in *Polymer Surfaces and Interfaces: Characterization, Modification and Applications*, (Ed.: M. Stamm) Springer, Berlin Heidelberg **2008**, pp. 215–234.
- [22] T. Ishikawa, M. Kobayashi, A. Takahara, *ACS Appl. Mater. Interfaces* **2010**, *2*, 1120.
- [23] X. He, W. Yang, X. Pei, *Macromolecules*. **2008**, *41*, 4615.
- [24] R. Gusain, S. Kokufu, P. S. Bakshi, T. Utsunomiya, T. Ichii, H. Sugimura, O. P. Khatri, *Appl. Surf. Sci.* **2016**, *364*, 878.
- [25] G. Yu, F. Zhou, W. Liu, Y. Liang, S. Yan, *Wear*. **2006**, *260*, 1076.
- [26] P. S. Bakshi, R. Gusain, O. P. Khatri, *RSC Adv.* **2016**, *6*, 78296.
- [27] W. Zhang, H. Yang, F. Liu, T. Chen, G. Hu, D. Guo, Q. Hou, X. Wu, Y. Su, J. Wang, *RSC Adv.* **2017**, *7*, 32518.
- [28] H. Fan, J. Wang, P. Wu, L. Zheng, J. Xiang, H. Liu, B. Han, L. Jiang, *Chem.* **2021**, *7*, 1852.
- [29] C. J. Clarke, L. Bui-Le, J. Hallett, *Anal. Methods*. **2020**, *12*, 2244.
- [30] T. Koishi, *J. Phys. Chem. B*. **2018**, *122*, 12342.
- [31] A. De los Rios, F. Hernández-Fernández, F. Tomás-Alonso, J. Palacios, D. Gómez, M. Rubio, G. Villora, *J. Membr. Sci.* **2007**, *300*, 88.
- [32] F. J. Hernández-Fernández, A. P. de los Ríos, F. Tomás-Alonso, J. M. Palacios, G. Villora, *AIChE J.* **2012**, *58*, 583.
- [33] J. Lemus, J. Palomar, M. A. Gilarranz, J. J. Rodriguez, *Adsorption*. **2011**, *17*, 561.
- [34] C. J. Clarke, S. Maxwell-Hogg, E. F. Smith, R. R. Hawker, J. B. Harper, P. Licence, *Phys. Chem. Chem. Phys.* **2019**, *21*, 114.
- [35] J. Chastain, R. C. King Jr, *Perk.-Elmer Corp.* **1992**, *40*, 221.
- [36] S. Seo, J. Park, Y. C. Kang, *Bull. Korean Chem. Soc.* **2016**, *37*, 355.
- [37] V. Palermo, M. Palma, P. Samori, *Adv. Mater.* **2006**, *18*, 145.
- [38] X. N. Zhang, H.-M. Hu, *Acta. Phys. Chim. Sin.* **2016**, *32*, 1722.
- [39] A. Dhotel, Z. Chen, J. Sun, B. Youssef, J.-M. Saiter, A. Schönhal, L. Tan, L. Delbreilh, *Soft Matter*. **2015**, *11*, 719.
- [40] R. Parmar, P. Lakhani, D. Bhandari, S. Kane, U. K. Goutam, C. K. Modi, *J. Organomet. Chem.* **2024**, *1008*, 123073.
- [41] J. Zenner, K. Tran, L. Kang, N. Kinzel, C. Werlé, S. DeBeer, A. Bordet, W. Leitner, *Chem.–Eur. J.* **2024**, *30*, 202304228.
- [42] N. Levin, L. Goclik, H. Walschus, N. Antil, A. Bordet, W. Leitner, *J. Am. Chem. Soc.* **2023**, *145*, 22845.
- [43] M. I. Qadir, M. V. Castegnar, F. F. Selau, D. L. Baptista, G. Chacon, R. B. Pontes, A. M. Lisboa, D. Eberhardt, J. Dupont, *Appl. Catal., B.* **2024**, *341*, 123315.
- [44] H. Meyer, M. Meischein, A. Ludwig, *ACS Comb. Sci.* **2018**, *20*, 243.
- [45] T. Torimoto, K. Okazaki, T. Kiyama, K. Hirahara, N. Tanaka, S. Kuwabata, *Appl. Phys. Lett.* **2006**, *89*.
- [46] S. Escolástico, C. Solís, C. Kjølseth, J. M. Serra, *ACS Appl. Mater. Interfaces*. **2017**, *9*, 35749.
- [47] A. C. P. M. Alves, L. M. N. B. F. Santos, M. Bastos, J. C. S. Costa, *Molecules*. **2023**, *28*, 3029.
- [48] L. Calabria, J. A. Fernandes, P. Migowski, F. Bernardi, D. L. Baptista, R. Leal, T. Grehl, J. Dupont, *Nanoscale*. **2017**, *9*, 18753.
- [49] G.-H. An, E.-H. Lee, H.-J. Ahn, *Phys. Chem. Chem. Phys.* **2016**, *18*, 14859.
- [50] S. J. Louis Anandaraj, L. Kang, S. DeBeer, A. Bordet, W. Leitner, *Small*. **2023**, *19*, 2206806.
- [51] L. Goclik, H. Walschus, A. Bordet, W. Leitner, *Green Chem.* **2022**, *24*, 2937.
- [52] H. Fujiwara, *Spectroscopic Ellipsometry: Principles and Applications*, John Wiley & Sons, Hoboken **2007**.
- [53] A. Paul, P. K. Mandal, A. Samanta, *J. Phys. Chem. B*. **2005**, *109*, 9148.
- [54] H. G. Tompkins, S. Tasic, J. Baker, D. Convey, *Surf. Interface Anal.* **2000**, *29*, 179.
- [55] V. H. Paschoal, L. F. Faria, M. C. Ribeiro, *Chem. Rev.* **2017**, *117*, 7053.
- [56] A. N. Parikh, D. L. Allara, I. B. Azouz, F. Rondelez, *J. Phys. Chem.* **1994**, *98*, 7577.
- [57] Y. Jeon, J. Sung, C. Seo, H. Lim, H. Cheong, M. Kang, B. Moon, Y. Ouchi, D. Kim, *J. Phys. Chem. B*. **2008**, *112*, 4735.
- [58] T. Garling, Y. Tong, T. A. Darwish, M. Wolf, R. K. Campen, *J. Phys.: Condens. Matter*. **2017**, *29*, 414002.
- [59] Y. Tong, J. Wirth, H. Kirsch, M. Wolf, P. Saalfrank, R. K. Campen, *J. Chem. Phys.* **2015**, *142*, 054704.
- [60] S. Nihonyanagi, S. Yamaguchi, T. Tahara, *J. Chem. Phys.* **2009**, *130*, 204704.
- [61] Y. Tong, E. Tyrode, M. Osawa, N. Yoshida, T. Watanabe, A. Nakajima, S. Ye, *Langmuir*. **2011**, *27*, 5420.
- [62] M. H. Valkenberg, C. deCastro, W. F. Hölderich, *Green Chem.* **2002**, *4*, 88.
- [63] V. Lockett, R. Sedev, C. Bassell, J. Ralston, *Phys. Chem. Chem. Phys.* **2008**, *10*, 1330.